Measurement of Muon Neutrino Charged-Current Neutral Pion Production at ICARUS

Lane Kashur

June 28, 2025

Abstract

Begin abstract

End abstract

Contents

1 Introduction

Serving as the far detector for the Short-Baseline Neutrino (SBN) Program, ICARUS is poised to address anomalous results from the LSND and MiniBooNE experiments, where excesses of electron-like events could possibly be interpreted as originating from light sterile neutrinos. One key to resolving these anomalies is the search for electron neutrinos in a predominantly muon neutrino beam, for which ICARUS and other detectors in the SBN suite rely on liquid-argon time projection chamber (LArTPC) technology. With excellent calorimetry and fine-grained spatial resolution, LArTPCs enable ICARUS to make precise measurements of electron neutrino interactions as part of a robust neutrino oscillation program.

Equally important to the success of ICARUS is characterization of backgrounds that can mimic the electron neutrino appearance signal. Primary among these backgrounds is the production of neutral pions, or π^0s, which decay electromagnetically to photons. π^0 production is mostly attributed to baryon resonance (RES) in neutrino-nucleon interactions that occur at few-GeV scale, which is also the energy at which the upcoming Deep Underground Neutrino Experiment (DUNE) neutrino beam peaks at. An ICARUS analysis centered around neutral pions therefore not only informs us about the SBN Program's

most significant background, but also provides a probe for the types of neutrino interactions expected at next-generation oscillation experiments.

1.1 Measurement

In this document, we report the measurement of muon neutrino charged-current interactions with a single π^0 in the final state on argon, hereafter referred to as ν_μ CC π^0 interactions:

$$\nu_\mu + Ar \rightarrow \mu^- + \pi^0 + 0\pi^\pm + X. \tag{1}$$

Here, X represents any final state particles that are not muons or charged pions. The ommitance of charged pions in the final state aims to exclude charged-current coherent pion production from the analysis, therefore allowing the cross section measurement to probe the resonant production mode that is more relevant to the SBN Program.

Few charged-current π^0 measurements exist on liquid argon, and a high statistics cross section measurment of this channel at ICARUS will help constrain uncertainties in modeling resonant neutrino-nucleuon interactions. We present single differential cross section measurements of ν_μ CC π^0 interactions as a function of muon and neutral pion kinematic variables, namely the momentum and angle with respect to the neutrino beam for each particle. Event selection is carried out with a novel machine-learning reconstruction pipeline known as SPINE, where high purity and excellent resolution in reconstructed variables enable the extraction of precise measurements. For information on the SPINE reconstruction chain, see Appendix B.

1.2 Data and Monte Carlo Samples

This analysis utilizes ICARUS data collected from the Booster Neutrino Beam (BNB) between winter 2022 and spring 2023 (ICARUS Run 2). This collection period corresponds to approximately 2.05×10^{20} protons on target (POT). The analysis can be easily extended to the Neutrinos at the Main Injector (NuMI) beam, and will be in the future as data processing and treatment of systematic uncertanties allows. Data is processed through the ICARUS reconstuction chain with *icaruscode* software version v09_89_01_02p01.

Monte Carlo simulation consisting of BNB neutrinos (produced with GENIE) and cosmics (produced with CORSIKA) is used to assess selection performance and evaulate systematic uncertainties. This includes a central value sample as well as dedicated detector variation samples, as will be discussed in Section 3. To evaluate the impact from cosmic activity that occurs within the 1.6 μs BNB beam gate, off-beam data is used. A summary of production streams used in this analysis is shown in Table 1.

Given its relevance to cross section measurements, the neutrino interaction model employed by GENIE merits further discussion. The Monte Carlo samples produced for this analysis use GENIE v3_04_00 with model configuration

AR23_20i_00_000. Commonly referred to as the SBN/DUNE tune, this configuration is widely used in ongoing analyses and is summarized in Table 2. Of particular interest to this analysis is the Berger-Sehgal resonance production model, as this yields the predicted number of neutral pions produced directly in ν-Ar interactions. Neutral pions can also be produced indirectly via final state interactions within the nucleus, in which case production rates are predicted by the INTRANUKE hA model.

Table 1: Data/simulation streams used for ν_μ CC π^0 analysis

Sample	Type	POT
BNB Run 2 On-Beam Majority Trigger	Data (on-beam)	2.05×10^{20}
BNB Run 2 Off-Beam Majority Trigger	Data (off-beam)	N/A
BNB ν + Cosmics	Simulation	1.32×10^{21}

Table 2: Summary of GENIE interaction model used for ν_μ CC π^0 analysis

Interaction	Model
Nuclear	Correlated Local Fermi Gas
Quasielastic Scattering	Valencia
2p2h	SuSAv2
Resonance	Berger-Sehgal
Coherent Pion Production	Berger-Sehgal
Deep Inelastic Scattering	Bodek-Yang
Hadronization	AGKY
Final State Interactions	INTRANUKE hA

1.2.1 Data and Beam Quality Cuts

Not yet implemented

To ensure the data used in this analysis is of physics quality, a number of data and beam quality cuts are enforced. Namely, any data collection runs that were subject to DAQ issues or happened during detector hardware updates are removed from consideration. Additionally, cuts are made to avoid detector features that are yet to be modeled in simulation, including a field cage short in the EE TPC and a cable hanging in the active volume of the WW TPC. A full description of all data and beam quality cuts used in this analysis can be found in Appendix A.

1.2.2 Unblinding Strategy and Timeline

The official blinding policy of the ICARUS collaboration (doc-db 34523) states that 90 percent of data is to remain blinded until any analysis is finalized. To comply with this policy, all analysis toward the ν_μ CC π^0 cross section measurement shown in this document only uses the 10 percent of Run 2 data

that has been unblinded. An exception has been made for data collection run 9435, which has been completely unblinded for the purpose of visual scanning.

A staged approach is taken for unblinding, with this technical note being updated and recirculated at each stage:

1. **Early summer 2025**: Submit technical note to collaboration. This submission serves to request access to the full ICARUS Run 2 BNB on-beam data set, corresponding to 2.05×10^{20} POT.
   (a) As a work-in-progress analsyis, a number of to-do items will continue to be focused on during this time.
   (b) Comments from the collaboration will be addressed before moving on to the next stage.
2. **Pending collaboration approval**: Unblind Run 2 on-beam data set and update relevant plots in this document. As part of this stage, updated distributions will be scrutinized to ensure unblinding did not introduce any new discrepancies or bugs.
3. **Late summer 2025**: Perform GUNDAM fitter studies, including closure tests that ensure fitter inputs are valid and p-value tests for goodness of fit.
4. **Early fall 2025**: Extract cross sections and report results to collaboration.

2 ν_μ CC π^0 Selection

2.1 Signal Definition

The ν_μ CC π^0 signal definition encompasses charged-current neutrino interactions occuring within the fiducial volume of the detector and containing

- exactly one primary muon ($p_\mu \geq 226$ MeV/c)
- exactly zero primary charged pions ($E_{\pi^\pm} \geq 25$ MeV)
- exactly one primary neutral pion
- any number of particles that are not muons or pions.

The momentum/energy requirements for muons and charged pions are phase space constraints to ensure tracking thresholds are met and purity is optimized. This signal definition applies to final state particles, or particles exiting the target nucleus post-final state interactions (FSI). The fiducial volume requirement applies to the neutrino interaction vertex, which must be 25 cm from detector boundaries in the drift and vertical directions, 30 cm from the upstream detector face, and 50 cm from the downstream face.

2.2 Selection Cuts

When selecting ν_μ CC π^0 interactions, cuts are made on various reconstructed outputs to narrow the list of candidate interactions. Included are cuts on:

- Fiducial volume: Reconstructed vertex is required to be inside fiducial volume (defined in signal definition).
- Flash time: Interaction is associated with an optical flash that is in-time with BNB beam gate, as determined by the OpT0Finder algorithm.
- Base Topology: Interaction contains
  - Exactly one primary muon ($p_\mu \geq 226$ MeV/c)
  - Exactly zero primary charged pions ($E_{\pi^\pm} \geq 25$ MeV)
  - Two or three primary photons ($E_\gamma \geq 20$ MeV)
- Leading Photon: Highest energy photon has $E_\gamma \geq 40$ MeV
- Neutral pion mass: Invariant diphoton mass < 400 MeV in order to reject η mesons.

Note that in the case of three primary photons meeting the above selection criteria, the photon pair with diphoton invariant mass closest to that of the true π^0 mass is chosen to belong to the candidate π^0.

2.3 Selection Performance

Selection performance is assessed using the BNB ν + Cosmic MC sample and off-beam BNB Run 2 data. The metrics that have been evaulated are efficiency - the fraction of true signal interactions that are matched to selected interactions, and purity - the fraction of selected interactions that are matched to true signal interactions. Efficiency and purity for each selection cut are shown in Table 3.

Table 3: Purity and efficiency for ν_μ CC π^0 Selection Cuts

Selection Cut	Efficiency [%]	Purity [%]
No Cut	100.0	0.0
In-Time Flash	97.1	0.5
Fiducial Volume	96.6	2.6
Base Topology	71.6	80.7
Leading Shower	71.6	81.1
$m_{\gamma\gamma} < 400$ MeV/c^2	**71.5**	**82.6**

Selection efficiency as a function of the cross section variables introduced in Section 1 are shown in Figure 1, showing that efficiency is largely flat across the signal phase space. Both inefficiencies and impurities in the selection are driven by particle identification (PID) failures, as shown in the particle identification

confusion matrix for true signal particles in Figure 2 and the histograms for reconstructed observables in Section 2.4.

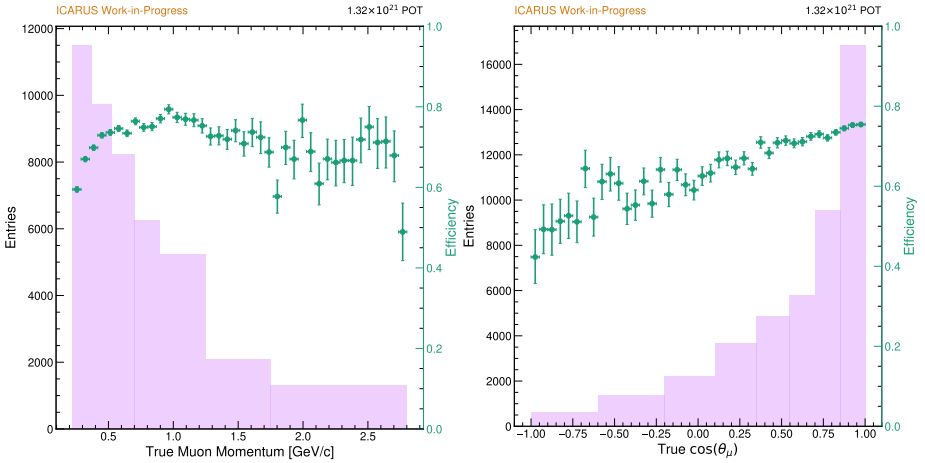

(a) True muon momentum.

(b) True $\cos\theta_{\mu}$.

(c) True neutral pion momentum.

(d) True $\cos\theta_{\pi^0}$.

Figure 1: Selection efficiency as a function of kinematic variables

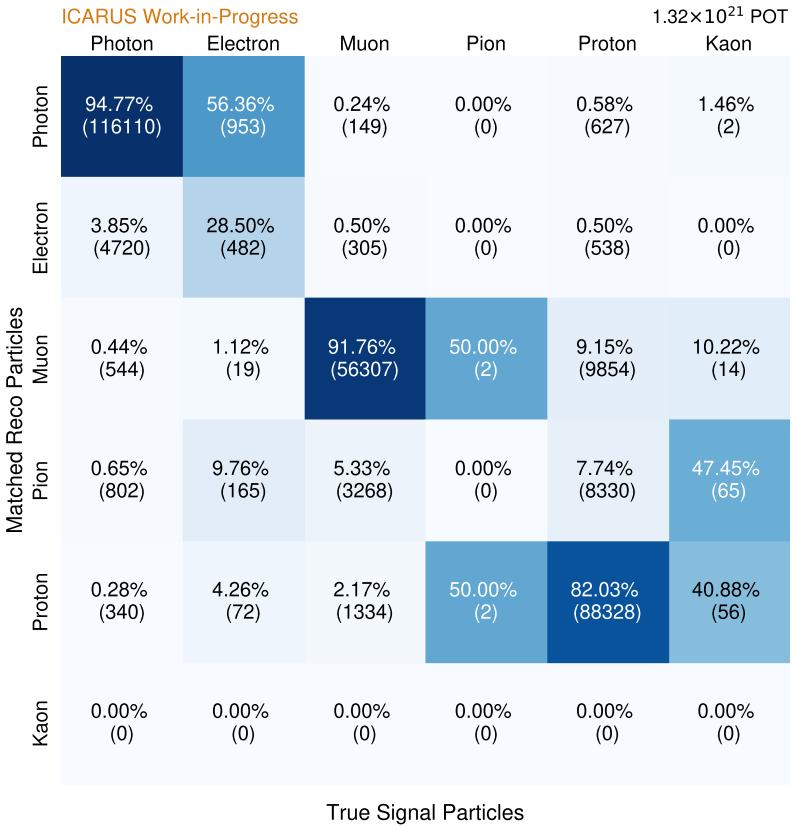

Figure 2: Particle identification confusion matrix for signal ν_μ CC π^0 interactions, as determined by the SPINE machine learning reconstruction chain.

2.4 Reconstructed Observables

In this section, the kinematic observables used in the single differential cross section measurement are highlighted. Included are the momenta of the final state muon and neutral pion, as well as the angles these particles make with the BNB. An additional variable, the invariant diphoton mass, is examined as it serves as a useful standard candle in the calibration of the electromagnetic shower energy scale.

For each case, the high purity of the selection is shown, with interactions containing one muon, zero charged pions, and one neutral pion ($1\mu 0\pi^{\pm} 1\pi^0$) being the dominant contribution at $\sim 83\%$. Among the background categories considered are $1\mu 0\pi^{\pm} 1\pi^0$ interactions where at least one particle fails the phase space requirements of the signal definition (out of phase space or OOPS) and $1\mu 0\pi^{\pm} 1\pi^0$ interactions that fail the fiducial volume requirement of the signal definition (out of fiducial volume or OOFV). If these interactions are allowed to pass the selection, the selection purity increases to $\sim 84\%$. Other backgrounds

include $1\mu\mathrm{N}\pi^{\pm}1\pi^{0}$ interactions that contain at least one charged pion (typically misreconstructed as a proton) and "Other ν" interactions featuring topologies that don't meet the requirements of the other listed background categories, such as those containing nonprimary neutral pions from secondary scattering.

2.4.1 Muon Observables

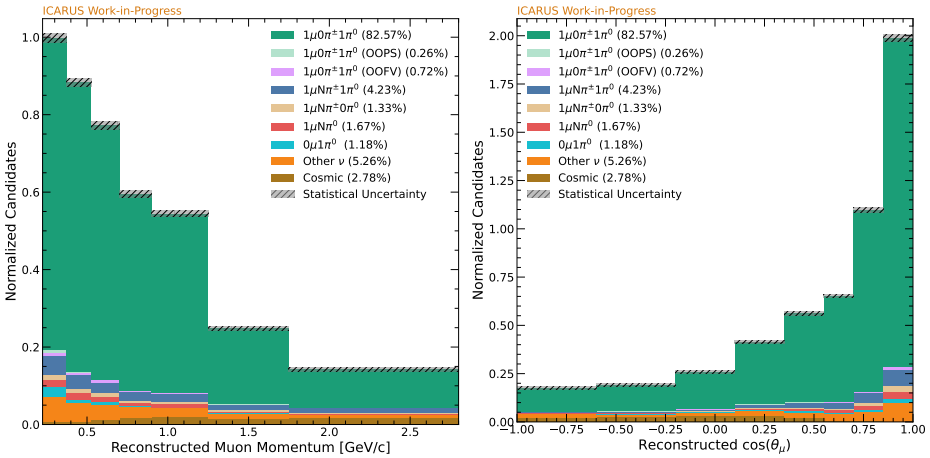

(a) Muon momentum (b) Muon angle with respect to neutrino beam

Figure 3: Muon observables chosen for analysis

2.4.2 Neutral Pion Observables

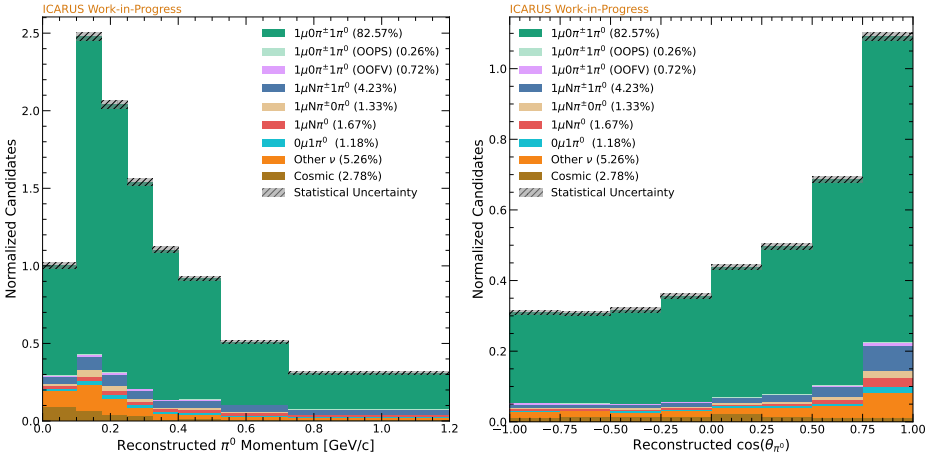

(a) Neutral pion momentum

(b) Neutral pion angle with respect to neutrino beam

Figure 4: Neutral pion observables chosen for analysis

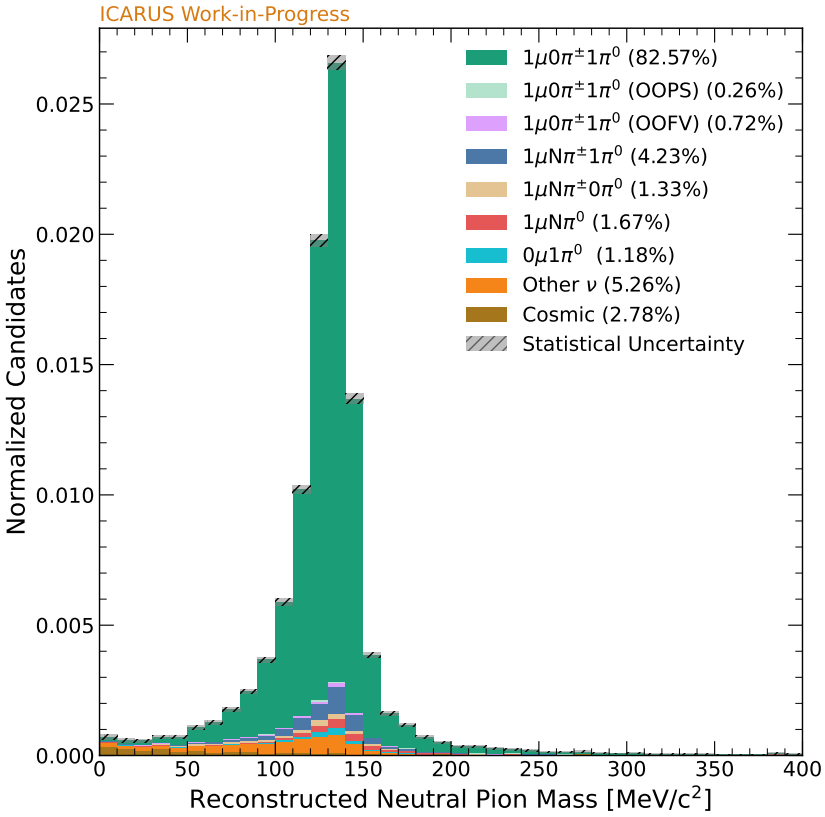

Figure 5: Neutral pion invariant mass

2.4.3 Transverse Kinematic Imbalance Observables

Transverse kinematic imbalance (TKI) variables are commonly studied in cross section analyses given their sensitivity to nuclear effects like FSI. The following TKI observables are examined:

$\delta\mathbf{p_T}$ Transverse momentum imbalance, or the magnitude of the vector difference between the transverse momentum of the muon and the hadronic system

$\delta\boldsymbol{\alpha_T}$ Transverse boosting angle, or the angle between the transverse momentum imbalance vector and the negative transverse momentum of the muon

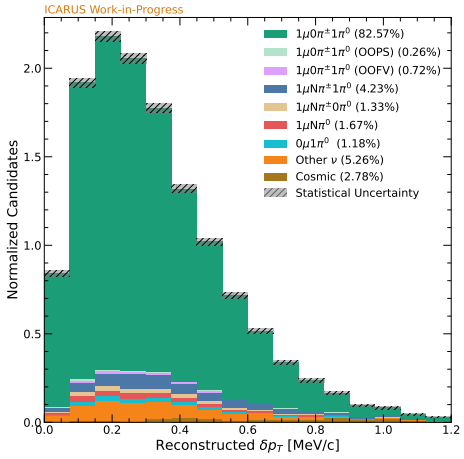

(a) Transverse momentum imbalance

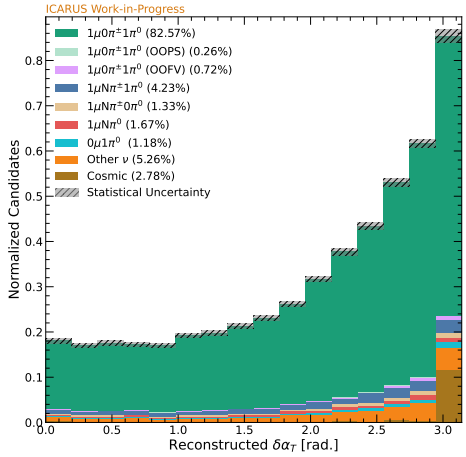

(b) Transverse boosting angle

Figure 6: Transverse kinematic imbalance observables

3 Systematic Uncertainties

The systematic uncertanties relevant to this analysis are divided into three categories: (1) beam flux, (2) interaction modeling, and (3) detector response modeling. Beam flux and interaction modeling uncertainties are evaluated through event reweighting using either a multisim, multisigma, or morph technique. With each approach, parameters affecting the probability of an interaction occuring are varied in a number of "universes". One thousand universes are employed in this analysis, each of which is used to assign weights to neutrino interactions in order to assess the impact of the parameter variations. A covariance

matrix then captures the uncertainty on binned reconstructed observables by comparing event counts across different universes and the central value sample:

$$V_{ij} = \frac{1}{N}\sum_{k}^{N}(M_i^k - M_i^{CV})(M_j^k - M_j^{CV}) \tag{2}$$

where N is the number of universes, M_i^k (M_j^k) is the measured event count for bin i (j) in the kth universe, and M_i^{CV} (M_j^{CV}) is the measured event count for bin i (j) in the central value universe.

Detector response modeling uncertainties are evaluated with a "uni-sim" technique, where elements of the detector response model are modified in dedicated variation samples. For every bin of a reconstructed observable, the ratio of events in the variation sample to events in the central value sample is represented in a spline that varies according to the number of standard deviations away from the nominal detector model parameter. The spline is then evaluated for every selected interaction in a configurable number of universes (10,000 by default) defined by randomly thrown standard deviations. Covariance matrix construction then follows in a manner analogous to the many-universes approach described previously.

3.1 Flux Uncertainties

The BNB flux at ICARUS is based on predictions from the MiniBooNE collaboration, which used the Geant4 simulation tool kit to model the propagation of particles produced in proton beam-target interactions [1]. Treatment of flux uncertainties, which arise from sources like hadron production, hadronic secondary interactions within the beam target, and beam focusing, are handled with a many-universes technique. The full set of beam flux uncertainties studied in this analysis are shown in Table 4.

Table 4: Flux uncertainties for ν_μ CC π^0 selection

Variation	Description	Uncertainty [%]
kminus	K^- production in beam target	0.01
kplus	K^+ production in beam target	0.63
kzero	K^0 production in beam target	0.03
piminus	π^- production in beam target	0.16
piplus	π^+ production in beam target	5.34
expskin	Current induced on surface of focusing horn	6.26
horncurrent	Current pulsed through focusing horn	0.79
nucleoninexsec	Nucleon inelastic re-scattering in beam target	0.80
nucleonqexsec	Nucleon QE re-scattering in beam target	2.48
nucleontotxsec	Nucleon total re-scattering in beam target	0.70
pioninexsec	π inelastic re-scattring in beam target	1.29
pionqexsec	π QE re-scattering in beam target	0.86
piontotxsec	π total re-scattering in beam target	0.99
Total		8.91

3.2 Interaction Model Uncertainties

Neutrino-argon interactions are simulated with the GENIE neutrino event generator, specifically version 3.4 with model configuration AR23_20i_00_00 - known colloquially as the "DUNE tune". GENIE provides reweightable parameters that can be used to assess interaction model uncertainties via the many-universes approach, similar to the handling of flux uncertainties discussed previously. The full set of interaction model uncertainties studied in this analysis are shown in Tables 5 and 6.

Table 5: Multisim interaction model uncertainties for ν_μ CC π^0 selection

Variation	Description	Uncertainty [%]
ZExpAVariationResponse	Z-expansion of axial form factor for CCQE interactions	2.12
NCELVariationResponse	Variation of the dipole form factor for NCEL interactions	0.03
CCRESVariationResponse	Variation of the dipole form factor for CCRES interactions	20.15
NCRESVariationResponse	Variation of the dipole form factor for NCRES interactions	0.32
DISBYVariationResponse	Variation of parameters in Bodek-Yang DIS model	0.08
FSI_pi_VariationResponse	Variation of FSI parameters involving pions	21.58
FSI_N_VariationResponse	Variation of FSI parameters involving nucleons	0.84
Total		29.61

Table 6: Multisigma interaction model uncertainties for ν_μ CC π^0 selection

Variation	Description	Uncertainty [%]
RPA_CCQE	RPA supression for CCQE interactions	2.51
CoulombCCQE	Value of Coulomb potential in corrections for CCQE interactions	0.05
NormCCMEC	Normalization for CCMEC interactions	0.93
NormNCMEC	Normalization for NCMEC interactions	0.01
NonRESBGvpCC1pi	Scale factor for non-resonant ν-p CC 1π background	0.21
NonRESBGvpCC2pi	Scale factor for non-resonant ν-p CC 2π background	3.04
NonRESBGvpNC1pi	Scale factor for non-resonant ν-p NC 1π background	0.02
NonRESBGvpNC2pi	Scale factor for non-resonant ν-p NC 2π background	0.25
NonRESBGvnCC1pi	Scale factor for non-resonant ν-n CC 1π background	2.73
NonRESBGvnCC2pi	Scale factor for non-resonant ν-n CC 2π background	4.68
NonRESBGvnNC1pi	Scale factor for non-resonant ν-n NC 1π background	0.08
NonRESBGvnNC2pi	Scale factor for non-resonant ν-n NC 2π background	0.14
NonRESBGvbarpCC1pi	Scale factor for non-resonant $\bar{\nu}$-p CC 1π background	0.02
NonRESBGvbarpCC2pi	Scale factor for non-resonant $\bar{\nu}$-p CC 2π background	0.04
NonRESBGvbarpNC1pi	Scale factor for non-resonant $\bar{\nu}$-p NC 1π background	0.00
NonRESBGvbarpNC2pi	Scale factor for non-resonant $\bar{\nu}$-p NC 2π background	0.00
NonRESBGvbarnCC1pi	Scale factor for non-resonant $\bar{\nu}$-n CC 1π background	0.00
NonRESBGvbarnCC2pi	Scale factor for non-resonant $\bar{\nu}$-n CC 2π background	0.05
NonRESBGvbarnNC1pi	Scale factor for non-resonant $\bar{\nu}$-n NC 1π background	0.00
NonRESBGvbarnNC2pi	Scale factor for non-resonant $\bar{\nu}$-n NC 2π background	0.01
RDecBR1gamma	Scale factor for $X + 1\gamma$ branching fraction	0.15
RDecBR1eta	Scale factor for $X + 1\eta$ branching fraction	2.75
NormCCCoh	Scale factor for CC coherent pion production	0.10
NormNCCoh	Scale factor for NC coherent pion production	0.00
Total		7.32

3.3 Detector Response Model Uncertainties

To assess systematic uncertainties involving the detector response model, ICARUS makes use of variation samples in which some element of the detector response simulation is modified from its nominal value. The intent of this approach is to characterize effects that are not fully modeled or understood. Elements of the detector response model that have been been varied for this analysis are:

- **Electron Lifetime**: The nominal electron lifetime value simulated in icaruscode is 3 ms. However, analysis of Run 2 cosmic muon data shows cryostat dependence, with an east cryostat lifetime of ∼4 ms and a west cryostat lifetime of ∼8 ms. For this reason, two variation samples in which the electron lifetime is varied were produced - one with 4 ms lifetime and another with 8 ms lifetime.

- **TPC Induction 1 Gain**: To account for intransparency of the first wire induction plane, a 15% variation is placed on the gain of this plane. The

variation is handled with two samples (minus and plus variations).

- **Recombination**: Electron-ion recombination is nominally simulated with the Modified Box Model, but recent studies have shown the amount of recombination to depend on track angle with the drift electric field. This is encapsulated with the ellipsoidal model of recombination, which has been simulated in a variation sample.

- **PMT QE**: A discrepancy exists between the amount of scintillation light collected by ICARUS PMTs and that simulated by the ICARUS optical model. A variation meant to cover this discrepancy has been produced in which the nominal PMT quantum efficiency is lowered from 7.3% to 4%.

- **YZ Nonuniformity**: Analysis of cosmic muon data has shown charge scale variations in the plane transverse to the drift elctric field (YZ-plane) due to wire plane intransparency. This YZ-dependence of the charge scale has been implemented in a variation sample.

- **TPC Noise**: Channel-by-channel variations of intrinsic and coherent noise were seen during Run 2 data collection. To account for this, variation samples in which intrinsic noise is varied by ±3.7% and coherent noise is varied by ±4.9% have been produced.

Table 7: Detector response modeling uncertainties for ν_μ CC π^0 selection

Variation	Description	Uncertainty [%]
High electron lifetime	Simulate electron lifetime of 8 ms	0.38
Low electron lifetime	Simulate electron lifetime of 4 ms	0.99
TPC induction 1 gain	Vary of first induction plain gain by ±15%	1.43
Recombination	Simulate recombination with ellipsoidal model	3.62
PMT QE	Decrease PMT quantum efficiency to 4%	0.23
YZ nonuniformity	Correct for YZ-dependence of charge scale	0.97
TPC intrinsic noise	Vary intrinsic noise component by ±3.7%	0.46
TPC coherent noise	Vary coherent noise component by ±4.9%	0.31
Total		4.19

3.4 Summary of Systematic Uncertainties

The reconstructed observables chosen for this analysis are shown in Figure 7 with full systematic and statistical uncertainty included. A breakdown of the categories contributing to the overall uncertainty is also presented in Table 8.

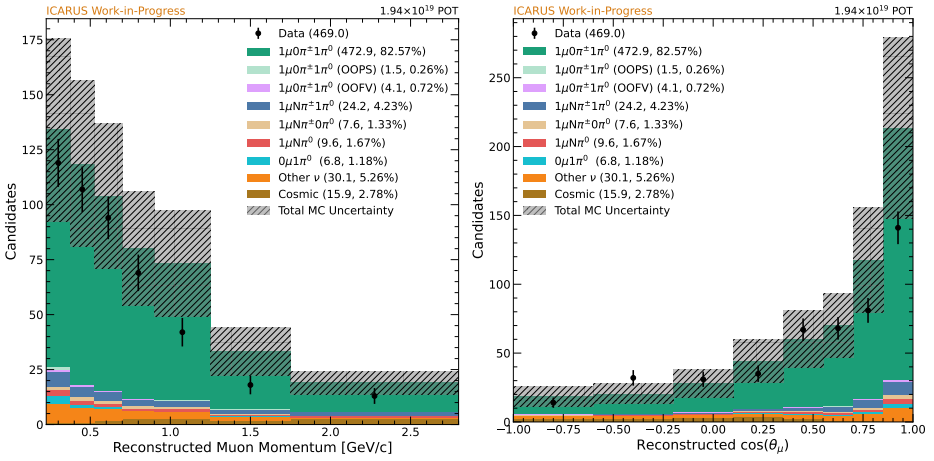

(a) Muon momentum

(b) Muon angle with respect to neutrino beam

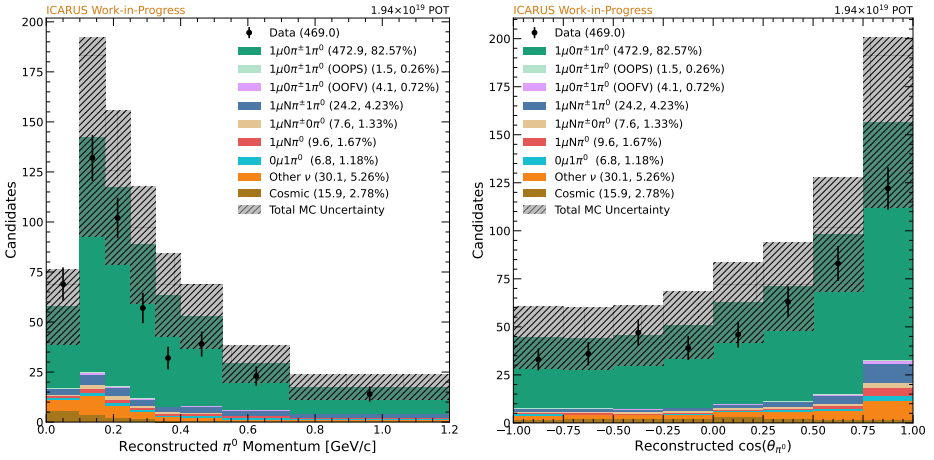

(c) Neutral pion momentum

(d) Neutral pion angle to neutrino beam

Figure 7: Observables chosen for analysis with full systematic uncertainty assessment

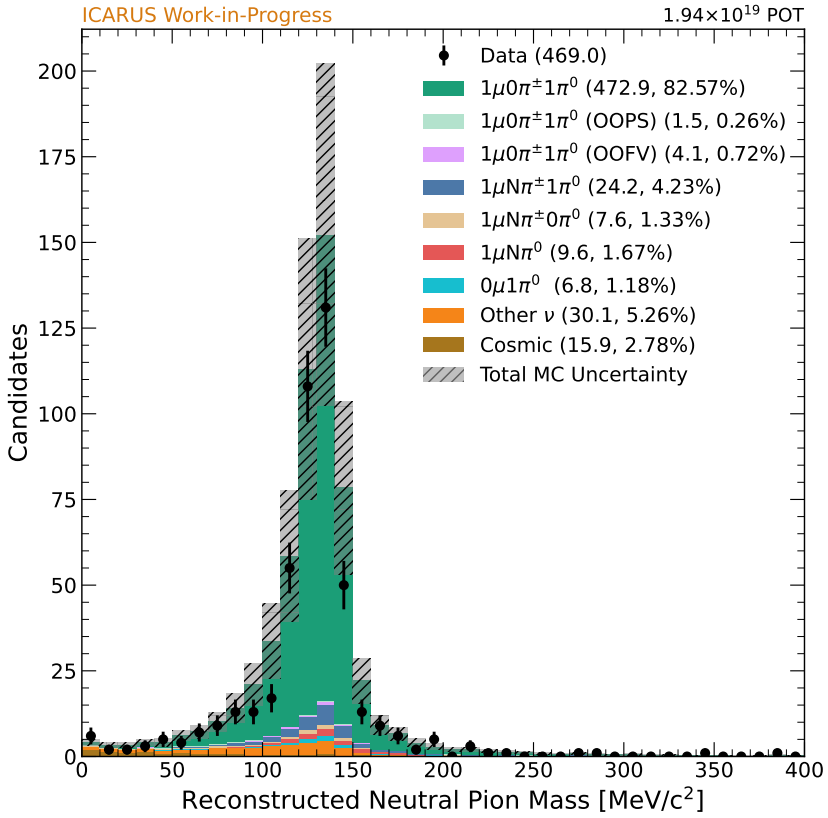

Figure 8: Neutral pion invariant mass with full systematic error assessment

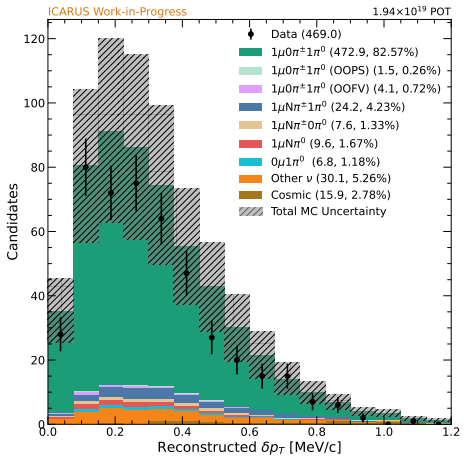

(a) Transverse momentum imbalance

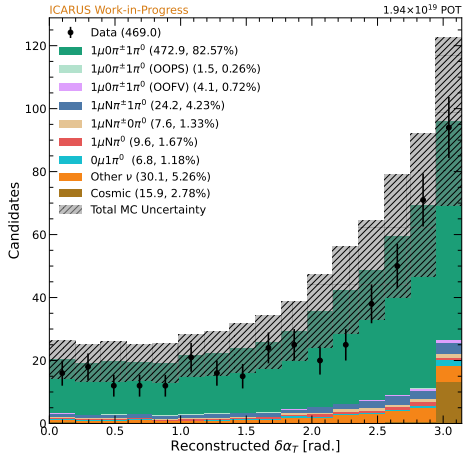

(b) Transverse boosting angle

Figure 9: Kinematic imbalance observables with full systematic uncertainty assessment

Table 8: Breakdown of uncertainties for ν_μ CC π^0 selection

Category	Uncertainty [%]
MC Statistical	0.51
Offbeam Statistical	8.64
Beam Flux	8.91
Interaction Model	30.50
Detector Response Model	4.19
Total	33.0

4 Cross Section Measurement

In a single differential cross section analysis, the dependence of the cross section on a specific variable is assessed. The measured cross section in true bin i of variable X is

$$\left.\frac{\mathrm{d}\sigma}{\mathrm{d}X}\right|_i = \sum_j \frac{U_{ij}(N_j - B_j)}{\Phi\ \epsilon_i\ N_{target}} \frac{1}{\Delta X_i}, \tag{3}$$

where j is a reconstructed bin, and N_j, B_j, and ϵ_j are the number of selected events, the number of background events, and the selection efficiency in bin j, respectively. X_i is the true bin width, while U_{ij} is an unfolding matrix that transofrms the background subtracted selected events in bin j to bin i. Φ is the integrated neutrino flux and N_{target} is the number of argon targets in the fiducial volume, both of which are discussed in the following subsection.

4.1 Input Preparation

4.1.1 Integrated Flux

The simulated BNB muon neutrino flux at the center of the ICARUS detector, scaled to the unblinded Run 2 POT, is shown in Figure 10. From this, the integrated neutrino flux through the face of the fiducial volume for unblinded Run 2 data is taken to be

$$\Phi = 8.25 \times 10^{09}\ \mathrm{cm}^{-2} \tag{4}$$

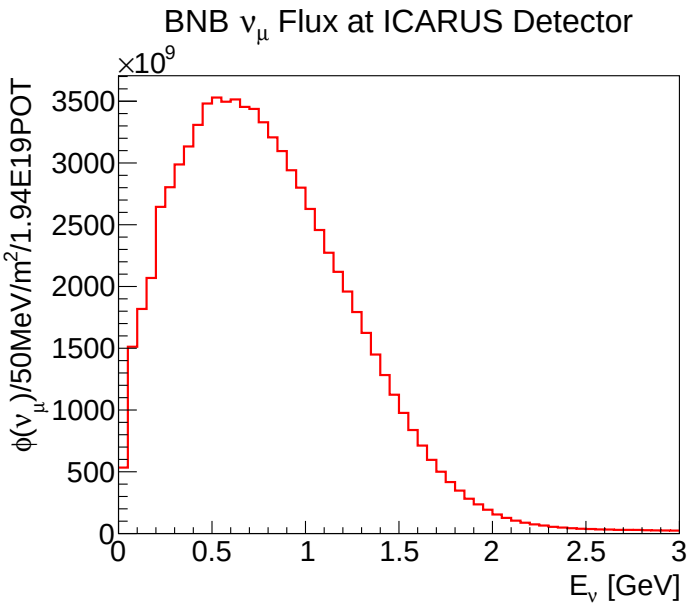

Figure 10: Muon neutrino flux at the ICARUS detector center, scaled to Run 2 unblinded POT.

4.1.2 Number of Targets

The number of fiducial nuclear argon targets, or N_{target}, is determined from the density of liquid argon ρ, the fiducial volume $V_{fiducial}$, and the atomic weight of argon M_{Ar}, and the number of nucleons per argon atom $N_{nucleons}$.

$$\begin{aligned} N_{target} &= \frac{\rho \cdot V_{fiducial} \cdot N_{nucleons}}{M_{Ar}} \\ &= \frac{1.39[\frac{\text{g}}{\text{cm}^3}] \cdot 2.25 \times 10^8[\text{cm}^3] \cdot 40}{6.63 \times 10^{-23}[\text{g}]} \\ &= 1.88 \times 10^{32} \text{ nucleons} \end{aligned} \tag{5}$$

4.2 Cross Section Extraction Procedure

Cross section measurements are carried out with the liklihood fitting and cross section extraction tool GUNDAM. As an open-source framework, GUNDAM was first designed for T2K analyses and has since been used for NuMI cross section measurements at ICARUS. This analysis marks the first use of GUNDAM in a BNB analysis.

To extract a cross section, the numerator of Equation (3), or the number of background-subtracted signal events for a given analysis bin after correcting for detector smearing, is first computed. This is achieved through binned liklihood

fitting, where template parameters controlling the number of Monte Carlo signal events in each analysis bin are varied such that the number of reconstructed Monte Carlo events best match observed counts from data. Nuissance parameters corresponding to flux, interaction, and detector systematic uncertainties are simultaneously considered in the fit.

After determining the number of signal events from the fit, Equation (3) is used to compute the differential cross section. To propagate uncertainty of the fit to the final cross section result, many universes are created in which best-fit parameters are varied within the uncertainties allowed by the post-fit covariance matrix. The cross section is recalculated for each universe, and the total uncertainty on the measurement is taken as the standard deviation across all universes.

4.3 Asimov Extraction

To demonstrate the GUNDAM cross section extraction machinery is functional and compatible with SPINE reconstructed output, an Asimov study in which selected event counts in data are assumed to be equal to those from Monte Carlo is carried out. Results are shown in Figure 11, and comparisons to the neutrino generator prediction will be made in Section 4.4.

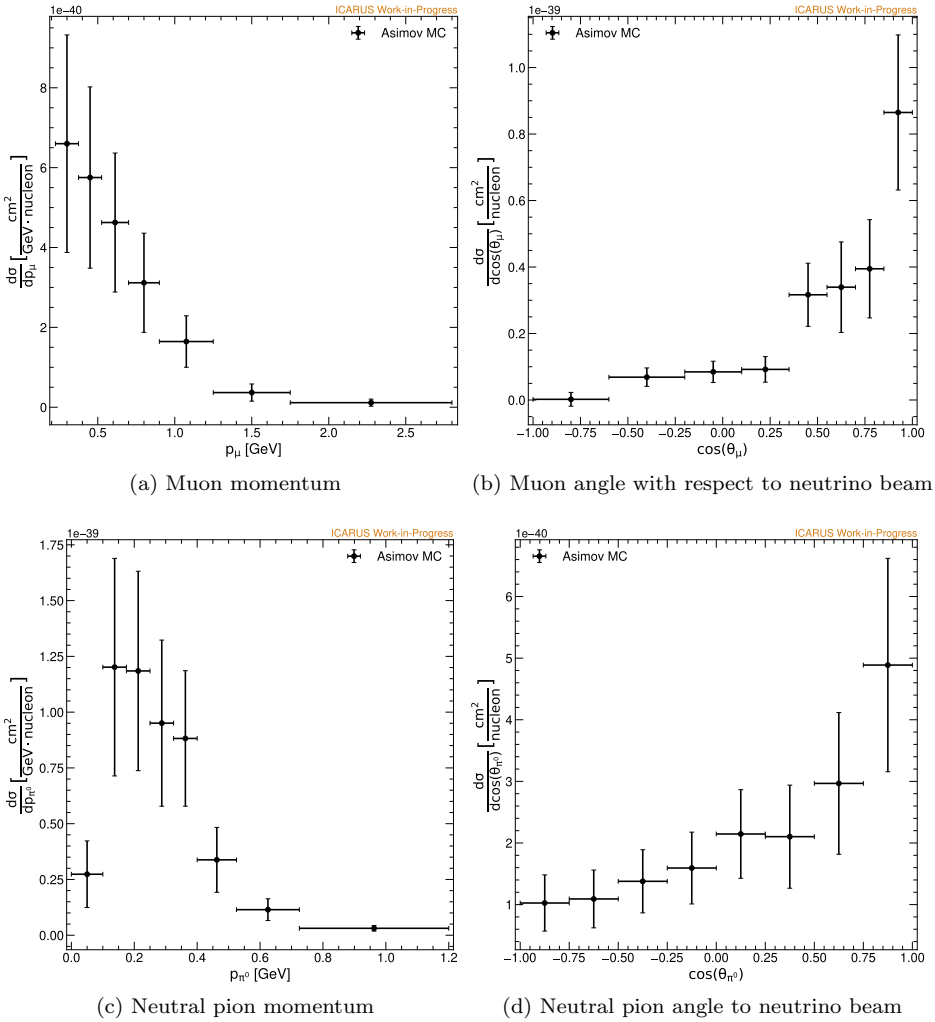

(a) Muon momentum

(b) Muon angle with respect to neutrino beam

(c) Neutral pion momentum

(d) Neutral pion angle to neutrino beam

Figure 11: Asimov cross section extraction for for analysis variables

4.4 Validation

To-do: Include closure tests, p-value tests, etc.

4.5 Results

5 Conclusions

References

[1] A. A. Aguilar-Arevalo et al. (MiniBooNE Collaboration), "Neutrino flux prediction at miniboone", Phys. Rev. D 79, 072002 (2009).

[2] F. Drielsma, K. Terao, L. Dominé, and D. H. Koh, "Scalable, end-to-end, deep-learning-based data reconstruction chain for particle imaging detectors", (2021).

Appendices

A Data and Beam Quality Cuts

A.1 Data Quality Cuts

To-do

A.2 Beam Quality Cuts

To-do

B Machine Learning Reconstruction

High-level reconstruction of neutrino events is handled by the end-to-end, machine-learning based reconstruction chain known as SPINE (Scalable Particle Imaging with Neural Embeddings) [2]. As input, SPINE takes an image of 3D charge depositions within the detector, which is then operated on by a series of neural networks to carry out point classification and formation of particle and interaction objects.

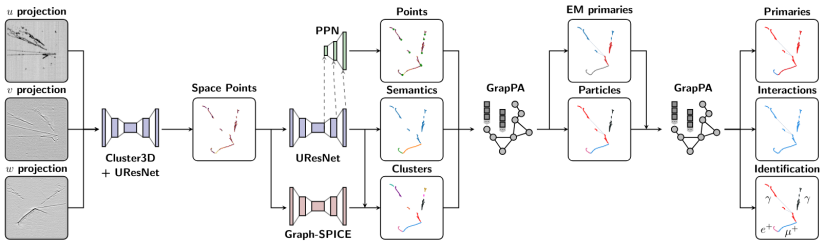

Figure 12: The SPINE reconstruction chain.

B.1 Point Classification

Point classification refers to the classification of 3D space points into abstract particle classes and the identification of points of interest. Convolution neural networks (CNNs) are used for these tasks, beginnining with the removal of tomographic reconstruction artifacts. Remaining space points are then assigned scores for the following semantic classes:

- **Electromagnetic showers** induced by electrons, positrons, and photons
- **Tracks**, including those from minimum ionizing and highly ionizing particles
- **Michel electrons** from the decay of muons
- **Delta ray** electrons from hard scattering of charged particles
- **Blips** from low-energy scattering

The semantic class with the highest score is the predicted particle-type for each voxel, and is used downstream in particle superstructure formation.

Within the UResNet architecture, additional convolutional layers are used to locate points of interest in each 3D image. Known as the Point Proposal Network (PPN), these convolutional layers are responsible for the prediction of track end points and shower start points. These quantities are then used as input for post-processing algorithms such as neutrino interaction vertex reconstruction, and are also used directly in the calculation of reconstructed variables like the invariant neutral pion mass.

A final task involving convolutional neural networks is dense clustering, or the density-based clustering of space points that belong to common semantic classes. For this, a UResNet architecture named Graph-SPICE is employed. Graph-SPICE applies a coordinate transformation to input space points such that clusters are disconnected, before a nearest-neighbor algorithm is taken to find connected components. The output of dense clustering is a collection of particle fragments for semantic types like tracks and showers.

B.2 Formation of Particles and Interactions

Following dense clustering, the next stage of SPINE reconstruction centers on the aggregation of particle fragments into complete track and shower objects. Unlike previous steps that were achieved with CNNs, the task of particle aggregation makes use of graph neural networks (GNNs) due to the natural graph-like representation of particles. Specifically, the Graph Particle Aggregator (GrapPA) network treats particle fragments (e.g. spatially separated shower fragments) as input graph nodes, and the correlations between them (e.g. the invisible photons connecting them) as input graph edges. By leveraging features of these nodes and edges, like PPN points and displacement vectors, GrapPA performs binary edge classification to group fragments belonging to the same

particle instance together. The result is a series of updated nodes and edges representing particle objects that can be used in the next stage of reconstruction.

With distinct particle objects in hand, particles that originate from the same neutrino interaction can be grouped together. Known as interaction aggregation, this task again uses GrapPA - now using particle instances as input graph nodes and the gaps between them as input graph edges. At this stage, nodes are also assigned scores for particle identification (also known as PID - the specific particle type) and primaryness (whether or not the particle originated from the neutrino vertex). PID classification includes photons, electrons, muons, pions, protons, and kaons, while primary classification is either primary or non-primary. The output of this stage, and the final output of SPINE's neural networks, is a set of interactions and the particles belonging to them.

C Energy Reconstruction

Energy reconstruction refers to the estimation of initial kinetic energy of particles in the ν_μ CC π^0 selection. From this, reconstructed observables like momentum can then be calculated.

C.1 Tracks

To estimate the energy of tracks made by charged particles (e.g. muons and charged pions), a "best estimate" approach is taken. For tracks contained within the active detector volume, energy is calculated using the Continous Slowing Down Approximation (CSDA) that relates a particle's kinetic energy to its range in a material. For energy estimation of exiting tracks, the degree of multiple coulomb scattering (MCS) along the track is instead used. Figure 13 shows how each energy estimate compares with true kinetic energy for simulated BNB muons from neutrino interactions.

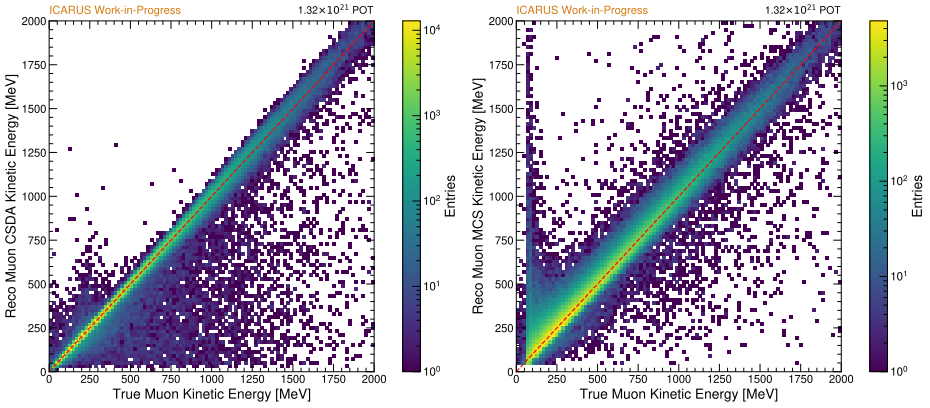

(a) CSDA Energy (b) MCS Energy

Figure 13: Track energy reconstruction for muons from BNB simulation

C.2 Showers

Unlike charged particles, neutral pions do not directly ionize the detector medium. The neutral pion energy must therefore be inferred from the electromagnetic showers instigated by the photons it decays to. Shower energy is estimated calorimetrically by summing charge depositions belonging to the shower and accounting for various detector effects:

$$E_{shower} = W_i[\frac{MeV}{e^-}] \cdot C_{cal}[\frac{e^-}{ADC}] \cdot C_{adj} \cdot \frac{1}{R} \cdot \sum_{dep} e^{\frac{t_{drift}}{\tau}} \cdot dep[ADC], \qquad (6)$$

where

W_i is the work function for argon

C_{cal} converts charge units from ADC to electrons

C_{adj} accounts for missing energy due to subthreshold charge and clustering effects in reconstruction

R is the recombination factor

τ is the electron lifetime

dep is charge in units of ADC.

The shower correction factor, C_{adj}, is derived from a study of contained photons in simulation. Figure 14a shows the ratio of reconstructed photon energy (from Equation 6) to true photon energy. As this ratio is mostly flat across different energies, a constant correction factor is chosen. Reconstructed photon energy is again compared to true photon energy in Figure 14b, showing agreement after the correction factor is applied. It is also worth noting that since the signal definition for this analysis does not require showers to be contained,

an additional correction factor is needed to correct for missing energy in exiting showers. A study for deriving this factor is ongoing with results expected soon.

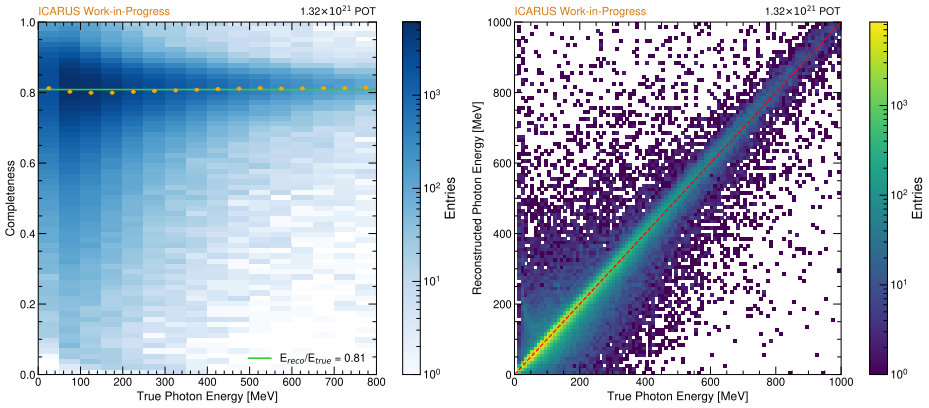

(a) Shower Energy Adjustment Factor (b) Post-Shower Energy Adjustment

Figure 14: Shower energy reconstruction for photons from BNB simulation